NASA/TM–2019–220282

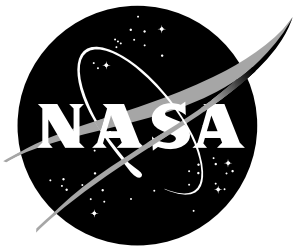

Mars Phoenix EDL Trajectory and Atmosphere Reconstruction Using NewSTEP

Christopher D. Karlgaard and Jake A. Tynis
Analytical Mechanics Associates, Inc., Hampton, Virginia

May 2019

NASA STI Program. . . in Profile

Since its founding, NASA has been dedicated to the advancement of aeronautics and space science. The NASA scientific and technical information (STI) program plays a key part in helping NASA maintain this important role.

The NASA STI Program operates under the auspices of the Agency Chief Information Officer. It collects, organizes, provides for archiving, and disseminates NASA's STI. The NASA STI Program provides access to the NASA Aeronautics and Space Database and its public interface, the NASA Technical Report Server, thus providing one of the largest collection of aeronautical and space science STI in the world. Results are published in both non-NASA channels and by NASA in the NASA STI Report Series, which includes the following report types:

- TECHNICAL PUBLICATION. Reports of completed research or a major significant phase of research that present the results of NASA programs and include extensive data or theoretical analysis. Includes compilations of significant scientific and technical data and information deemed to be of continuing reference value. NASA counterpart of peer-reviewed formal professional papers, but having less stringent limitations on manuscript length and extent of graphic presentations.
- TECHNICAL MEMORANDUM. Scientific and technical findings that are preliminary or of specialized interest, e.g., quick release reports, working papers, and bibliographies that contain minimal annotation. Does not contain extensive analysis.
- CONTRACTOR REPORT. Scientific and technical findings by NASA-sponsored contractors and grantees.
- CONFERENCE PUBLICATION. Collected papers from scientific and technical conferences, symposia, seminars, or other meetings sponsored or co-sponsored by NASA.
- SPECIAL PUBLICATION. Scientific, technical, or historical information from NASA programs, projects, and missions, often concerned with subjects having substantial public interest.
- TECHNICAL TRANSLATION. English-language translations of foreign scientific and technical material pertinent to NASA's mission.

Specialized services also include organizing and publishing research results, distributing specialized research announcements and feeds, providing information desk and personal search support, and enabling data exchange services.

For more information about the NASA STI Program, see the following:

- Access the NASA STI program home page at `http://www.sti.nasa.gov`
- E-mail your question to `help@sti.nasa.gov`
- Phone the NASA STI Information Desk at 757-864-9658
- Write to:
  NASA STI Information Desk
  Mail Stop 148
  NASA Langley Research Center
  Hampton, VA 23681-2199

NASA/TM–2019–220282

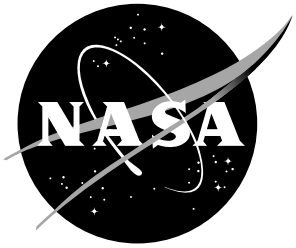

Mars Phoenix EDL Trajectory and Atmosphere Reconstruction Using NewSTEP

Christopher D. Karlgaard and Jake A. Tynis
Analytical Mechanics Associates, Inc., Hampton, Virginia

National Aeronautics and
Space Administration

Langley Research Center
Hampton, Virginia 23681-2199

May 2019

Acknowledgments

The content of this work benefited from discussions with Soumyo Dutta, Ashley Korzun, Rafael Lugo, Mark Schoenenberger, and Carlie Zumwalt.

Available from:

NASA STI Program / Mail Stop 148
NASA Langley Research Center
Hampton, VA 23681-2199
Fax: 757-864-6500

Abstract

This document describes the trajectory and atmosphere reconstruction of the Mars Phoenix Entry, Descent, and Landing using the New Statistical Trajectory Estimation Program. The approach utilizes a Kalman filter to blend inertial measurement unit data with initial conditions and radar altimetry to obtain the inertial trajectory of the entry vehicle. The nominal aerodynamic database is then used in combination with the sensed accelerations to obtain estimates of the atmosphere-relative state. The reconstructed atmosphere profile is then blended with pre-flight models to construct an estimate of the as-flown atmosphere.

1 Introduction

On May 28th, 2008 the Mars Phoenix lander successfully conducted its Entry, Descent, and Landing (EDL) sequence to land on the surface of Mars. Data from the on-board Inertial Measurement Unit (IMU) (accelerations and angular rates) and Orbit Determination (OD) initial conditions were utilized to reconstruct the as-flown trajectory of the entry vehicle from entry interface to touchdown using a dead reckoning integration technique. The nominal vehicle aerodynamic database was used to estimate the as-flown atmospheric density profile by solving for the density using the measured axial acceleration and the nominal axial force coefficient.

The methodology and results of the trajectory and atmospheric reconstruction are documented in [1] and [2]. Unfortunately, the reconstructed data has subsequently been lost. However, the raw telemetry data from the mission still exists and so can be used to reconstruct the trajectory and atmosphere for archival purposes. The reconstruction makes use of the New Statistical Trajectory Estimation Program (NewSTEP). NewSTEP is an Iterative Extended Kalman Filter (IEKF) [3] code for processing various types of on-board and ground-based (where applicable) measurements to produce a trajectory estimate that is a best fit to all of the data sources based on their given uncertainties.

This memorandum serves to document this reconstruction and the results. The remainder of the document is organized as follows. The next section provides a brief overview of the Phoenix entry vehicle and the nominal EDL timeline, and then gives an overview of the various measurement data sources that are used for the trajectory reconstruction. The following section provides an overview of the trajectory and atmosphere reconstruction methodology, before presenting the results of the reconstruction.

2 Vehicle Description

The Phoenix entry vehicle is a 70 deg sphere cone shape with a diameter of 2.65 m and mass at entry of 572.743 kg. The EDL concept of operations is shown in Figure 1. During the hypersonic phase the entry vehicle is unguided and is not spin stabilized. After peak heating and peak deceleration the vehicle slows to a Mach number of approximately 1.65 where the supersonic disk-gap-band parachute

is deployed. Shortly thereafter the heatshield is jettisoned, lander legs are deployed, the radar altimeter is activated, and the lander separates from the backshell and begins powered flight. During the terminal descent phase the lander flies on a gravity turn trajectory until reaching a condition close to the landing site, where it descends at a constant velocity until touchdown after which the motor is powered off. Additional details on the vehicle design and EDL system overview can be found in [4].

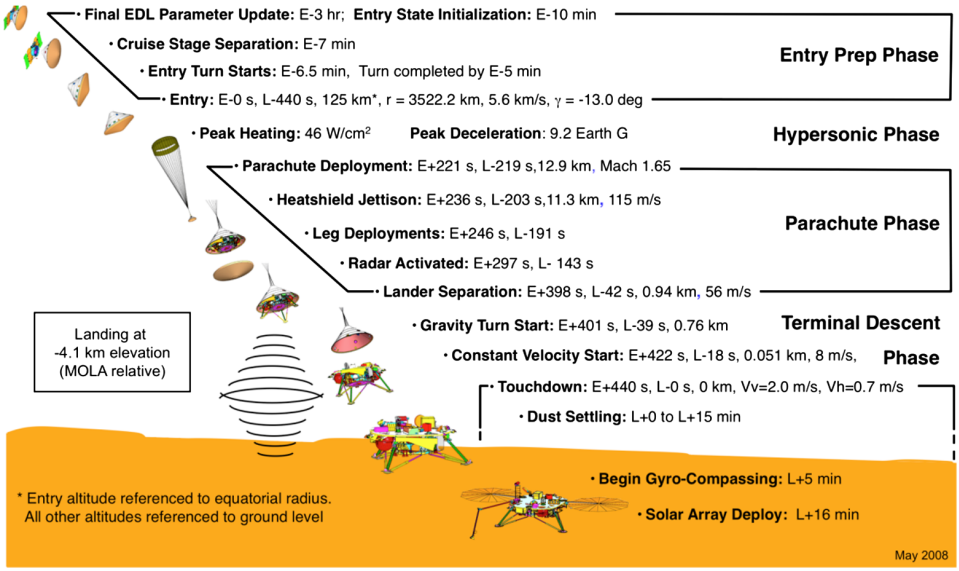

Figure 1: Phoenix Entry, Descent, and Landing

Coordinate frames relevant to the vehicle aerodynamics and flight mechanics are shown in Figure 2. The axes labeled X_C, Y_C, and Z_C are the axes of the cruise frame and the axes labeled X_B, Y_B, and Z_B define the flight mechanics body frame. Directions of the aerodynamic force coefficients C_A, C_Y, and C_N are shown relative to the flight mechanics body frame as are the definitions of the aerodynamic flow angles. The transformation from cruise frame to the flight mechanics body frame is given by

$$T_{cr2b} = \begin{bmatrix} 1 & 0 & 0 \\ 0 & 0 & -1 \\ 0 & 1 & 0 \end{bmatrix} \tag{1}$$

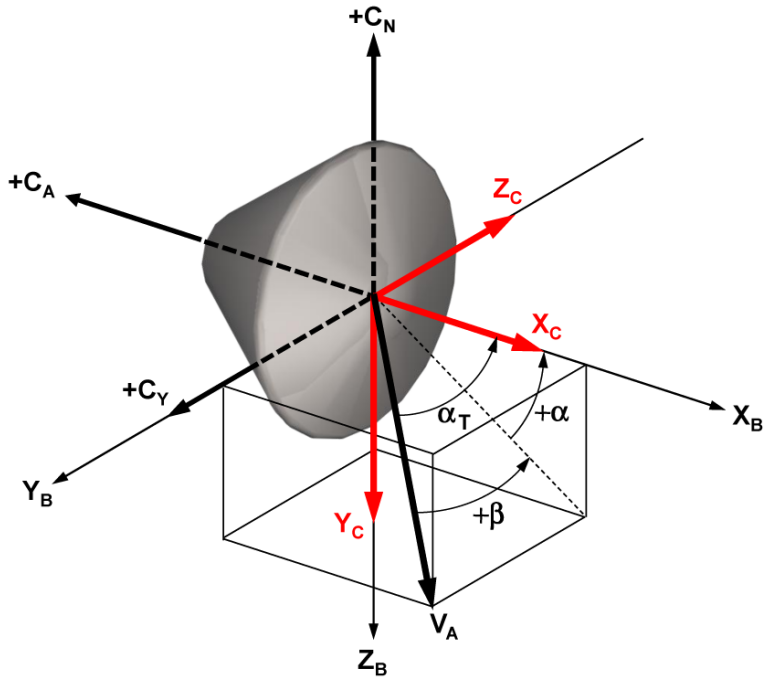

Figure 2: Phoenix Coordinate Frames

3 Data Sources

Several sources of measurement data are available to be used for trajectory reconstruction purposes. These include the IMU, radar altimeter, OD initial conditions, and the landing site position fix. Many of these data can be found in the "phx_tlm_v9.mat" MATLAB data file. The following subsections describe these data sources.

3.1 Inertial Measurement Unit

The primary measurement source for performing the trajectory and atmosphere reconstruction is the on-board IMU, which provides three axis linear acceleration and angular rate measurements in the IMU instrument frame. These measurements are provided at the rate of 200 Hz.

According to [1], the transformation from the IMU instrument frame to the cruise reference frame is given by the matrix

$$T_{imu2cr} = \begin{bmatrix} 0.001658000000000 & 0.434532000000000 & 0.900655000000000 \\ 0.865583671733631 & -0.451637796435926 & 0.216304845776395 \\ 0.500761102355330 & 0.779233610045474 & -0.37687298280806 \end{bmatrix} \tag{2}$$

The location of the IMU in the cruise reference frame is given by the vector $r_{imu} = \begin{bmatrix} 1.284866 & -0.5195119 & -0.228428 \end{bmatrix}^T$ m [1].

The measured accelerations were transformed from the IMU frame into the vehi-

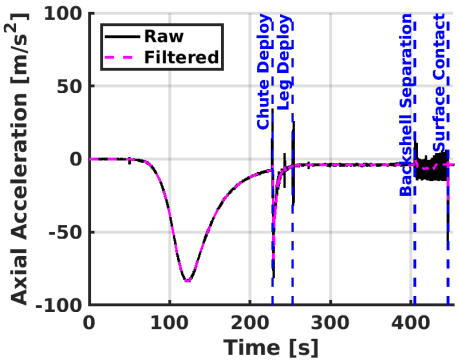

(a) Axial Acceleration

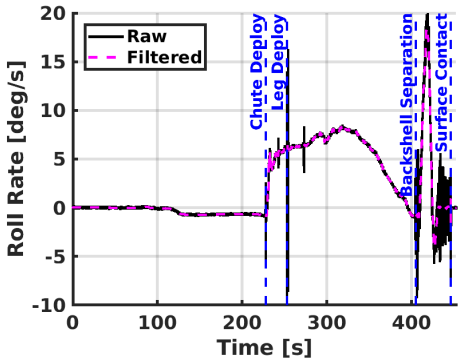

(b) Roll Rate

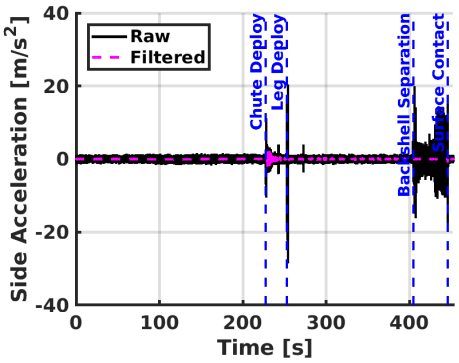

(c) Side Acceleration

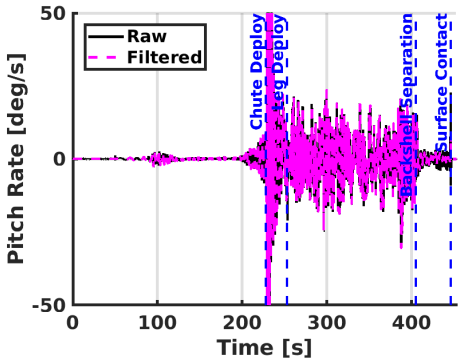

(d) Pitch Rate

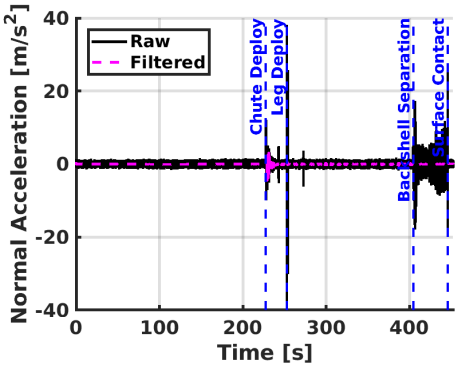

(e) Normal Acceleration

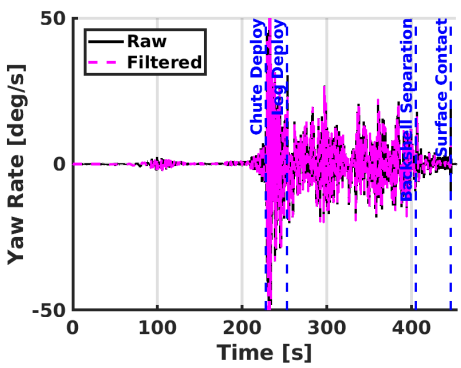

(f) Yaw Rate

Figure 3: Accelerations and Angular Rates in Flight Mechanics Body Frame

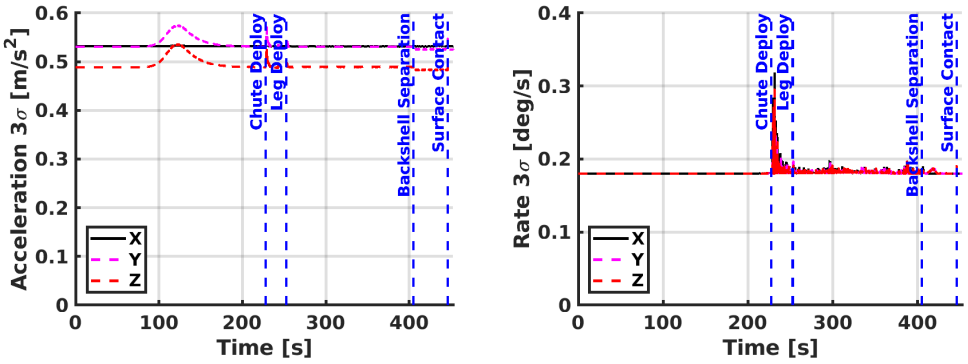

(a) Acceleration

(b) Angular Rate

Figure 4: Acceleration and Angular Rate Uncertainties

cle body frame for integration in order to propagate the states from the initial condition. The integration scheme accounts for the IMU position offset and transforms the accelerations to the vehicle center of mass. Note that the numerical integration of these data for propagating the vehicle state makes use of the raw accelerations with no filtering. A second-order Butterworth filter [5] with a 5 Hz cutoff frequency is also applied to smooth the data for use in the atmospheric reconstruction. The filter is applied in forward/backward mode to eliminate phase loss. The raw and filtered data are shown in Figure 3.

3.2 Radar Altimeter

After heat shield separation, the on-board radar altimeter was activated to measure the above ground level altitude of the vehicle during the terminal landing phase. These measurements can be used in the trajectory reconstruction process to provide position data that can be processed by the Kalman filter to improve the trajectory estimate.

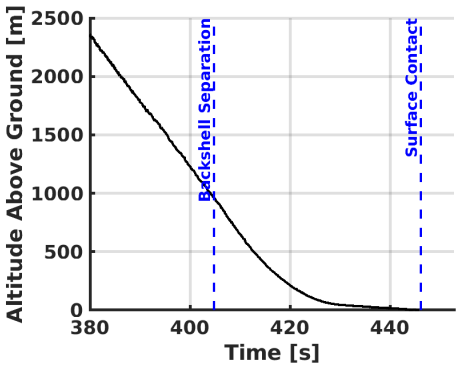

Figure 5: Radar Altimeter Data

The radar altimeter measurements are shown in Figure 5. The measurements are assumed to be accurate to 1% in scale factor error and 10 cm in random noise, in a 3σ sense.

3.3 Initial Conditions

The initial conditions used for the reconstruction are based on the orbit determination (OD) solution OD77 [6]. The states are provided in the Earth Mean Equator of January 2000 (EMEJ2000) [7] inertial frame at a spacecraft clock time (SCLK) of $t_0 = 896225523.896$ s. These coordintes correspond to a radius from the center of the planet of 3522.194 km. The position and velocity components are listed in Table 1. The initial condition covariance matrix is based on the initial condition uncertainties provided in [2], transformed into the appropriate coordinate frame. It is assumed that the uncertainties are uncorrelated.

Table 1: EMEJ2000 Orbit Determination 77 Initial Conditions

Coordinate	Initial Condition
X, m	1060304.16809705
Y, m	-645136.486623493
Z, m	3296270.9865079
$\dot{X}$, m/s	1464.27469596023
$\dot{Y}$, m/s	5350.16886003297
$\dot{Z}$, m/s	-770.68622121074

Similarly, the attitude initial conditions can be extracted from the OD77 navigation state contained within the Phoenix telemetry data. The attitude is based on a star tracker initialization prior to cruise stage separation that is then propagated forward in time based on the IMU gyroscope measurements. The attitude conditions at t_0 are listed in Table 2. The 3σ uncertainties are assumed to be 0.25 deg in each axis, uncorrelated.

Table 2: EMEJ2000 Cruise Frame Attitude Initial Conditions

Quaternion	Initial Condition
e_0	0.484415890110281
e_1	0.627367398405513
e_2	0.523106641741869
e_3	0.313226490246446

The initial orientation of Mars with respect to the EMEJ2000 frame is also required in order to compute the planet-relative trajectory. The Mars Centered

Mars Fixed (MCMF) frame is defined relative to the EMEJ2000 frame at t_0 by the quaternion listed in Table 3.

Table 3: EMEJ2000 MCMF Frame Initial Conditions

Quaternion	Initial Condition
e_0	0.414943021388918
e_1	2.39260776718649e-05
e_2	5.51686127775915e-05
e_3	-0.909847396756512

Note that these initial conditions differ slightly from those assumed in [1], though there is a time offset of approximately 68 ms (OD77 initial conditions occurred shortly after the conditions from [1]). The specific numbers assumed in [1] are not found in the provided Phoenix telemetry data structures that are used in the present analysis.

3.4 Landing Site Location

The Phoenix landing site location was extracted from the flight data file and is repeated in Table 4. This location is used for trajectory reconstruction purposes to provide an end point to the trajectory as another form of a position fix. The landing site location and associated uncertainties were determined from Doppler tracking [8]. This landing site corresponds to a Mars Orbiter Laser Altimeter (MOLA) elevation of -4131 m [8].

Table 4: Phoenix Landing Site Coordinates

Coordinate	Value	3σ
Radius	3376291.5 m	4.2 m
Longitude	234.24843 deg	0.000288 deg
Declination	68.21878 deg	0.00018 deg

Note that these coordinates are within 0.5 m of those specified in [1]. The difference is primarily in the longitude component with [1] providing a value $2.03 \cdot 10^{-5}$ deg larger.

3.5 Mass Properties Model

The mass properties models are based directly on those provided in [1] along with a timing adjustment to account for the 68 ms offset between the t_0 time definitions. The mass properties are referenced to SCLK time, but the time from t_0 is provided for convenience. The center of mass coordinates are specified in the cruise reference frame. The aerodynamic reference length, b is also provided in this table.

Table 5: Phoenix Mass Properties

Event	$t - t_0$, s	X_{cm}, m	Y_{cm}, m	Z_{cm}, m	m, kg	b, m
Initialization	0.0	1.066129	0.000164	0.000010	572.74	2.65
Chute Deploy	227.7	1.080957	0.000168	0.000010	572.74	11.8
Heatshield Jettison	242.7	1.045280	-0.000642	0.001535	510.62	11.8
Leg Deployment	252.7	1.061298	-0.000642	0.001535	510.62	11.8
Backshell Separation	404.8	1.14807	-0.000611	0.00076	400.75	2.605
Surface Contact	446.1	1.146875	-0.000674	0.000854	363.19	2.605

3.6 Atmosphere Model

A preflight atmosphere model has been developed in using the Mars Regional Atmospheric Modeling System (MRAMS) [15] for the Phoenix landing site in [16]. This model include a nominal atmosphere profile and 2000 dispersed cases that were used for preflight trajectory Monte Carlo analysis such as that described in [17].

Atmospheric profiles for the Phoenix landing site were also directly measured using the Mars Climate Sounder (MSC) instrument [18] onboard the Mars Reconnaissance Orbiter (MRO). Atmosphere profiles based on MCS measurements were developed in support of landing day predictions. Profile 12, generated from data acquired on May 18th, was used for the final landing day prediction prior to actual landing [19]. The MCS continued to acquire data up to the actual landing day, and profile 21 was generated based on data 2 hours prior to landing on May 25th, representing the best available atmospheric profile [19]. Unfortunately these MCS profiles were not available for the purposes of this reconstruction, therefore the preflight nominal atmosphere was used as the initial guess for the atmosphere reconstruction.

One Sol after landing, measurements of the surface pressure and temperature were obtained by the Phoenix meteorological package [20] that can be used to provide in-situ atmospheric data [19]. Numerical values of these measurements were not found in the Phoenix telemetry data nor were recorded in the literature, however the data can be approximated from Figure 24(a) in [2], which indicates a surface temperature of 238 ± 5 K.

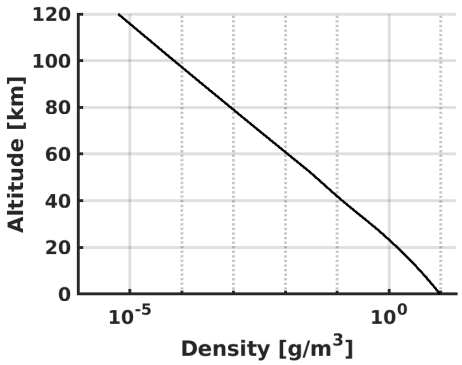

(a) Nominal Density

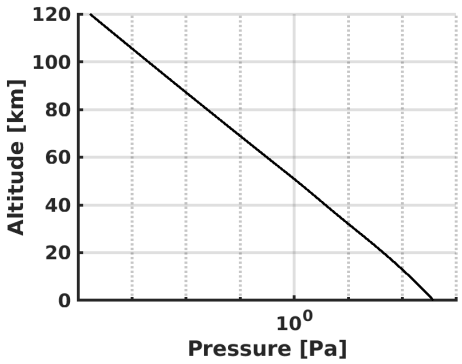

(b) Nominal Pressure

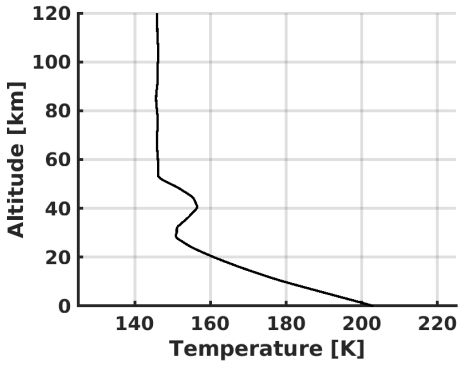

(c) Nominal Temperature

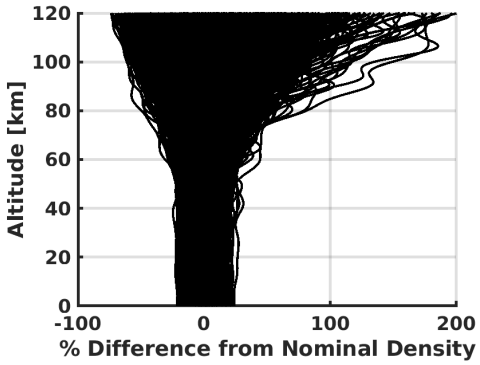

(d) Dispersed Density

Figure 6: Atmosphere Model

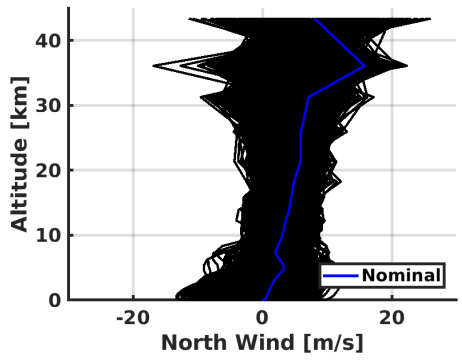

(a) North Wind

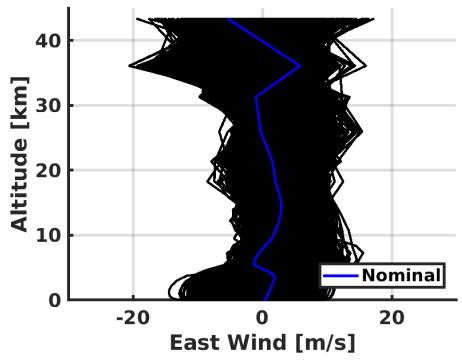

(b) East Wind

Figure 7: Winds Model

3.7 Aerodynamics Model

The aerodynamics model for the Phoenix entry vehicle was developed using a combination of historical data, previous flight tests of similar systems, wind tunnel testing, and computational methods. The Phoenix entry vehicle was geometrically similar to the Mars Exploration Rover, Pathfinder, and Viking geometries and leveraged this data as appropriate. This approach allowed an aerodynamic database to be generated that encompassed all of the flight regimes, including free molecular, transitional, hypersonic, supersonic, and transonic flows. The resultant database included static and dynamic coefficients along with associated uncertainties. The final aerodynamic database product is a model that can be queried with flight conditions and return the relevant aerodynamic coefficients for trajectory simulations. A detailed description and analysis of the Phoenix aerodynamic database can be found in [21].

3.8 Gravity Model

The Mars gravitational acceleration is modeled using the MRO110C model [22]. This model is based on tracking data of Mars Global Surveyor (MGS), Mars Odyssey and Mars Reconnaissance Orbiter (MRO), and MOLA-derived topography data. The model contains spherical harmonics up to degree and order 110.

4 Reconstruction Methods

The reconstruction process utilized for the Phoenix EDL data consists of three steps. In the first step, the NewSTEP code is used to generate a kinematic reconstruction of the inertial flight path of the vehicle based on Kalman filtering of the orbit determination initial conditions, IMU, Radar, and landing site coordinates. The nominal atmosphere profile is superimposed on this trajectory to produce a reasonable set of atmospheric-relative states. As part of this process, the measured IMU accelerations are transformed to the vehicle center of mass and rotated into the vehicle flight mechanics body coordinate frame.

In the next step, the nominal aerodynamic database and sensed accelerations are used to reconstruct the atmospheric-relative trajectory. Dynamic pressure is computed from the axial acceleration, mass, and reference area. The flow angles are simultaneously computed from the ratio of lateral to axial acceleration. The density is computed from the dynamic pressure and the reconstructed velocity (assuming the nominal winds), and then static pressure is computed from an integration of the hydrostatic equation. An estimate of the Mach number can be computed from the static and dynamic pressure. Uncertainties are also mapped through the process. The overall process is described in [14].

Note that the density reconstructed from the vehicle aerodynamics is only valid during the entry phase up until the point of parachute mortar fire. After parachute deployment, the vehicle aerodynamics are poorly known and so the atmosphere reconstruction must rely on another source. For this work, a pre-flight density profile was found that was a best fit to the reconstructed density in the altitude

range where the vehicle aerodynamics are well known. The density profile from the pre-flight model was anchored to the reconstructed density to provide an estimate of the density at altitudes below parachute deployment. The static pressure was computed from a top-down integration of the hydrostatic equation, and temperature was computed from the ideal gas law.

In the final step, another NewSTEP run was processed but instead of the pre-flight nominal atmosphere, the reconstructed atmosphere was superimposed on the trajectory in order to provide best estimates of the atmospheric-relative state from entry interface to touchdown.

5 Reconstruction Results

The results of the reconstruction process described in the previous section are shown in the following subsections, describing the inertial trajectory, atmospheric-relative trajectory, and the atmosphere reconstruction.

5.1 Inertial Trajectory

Components of the vehicle trajectory relative to the Mars surface are shown in Figure 8 along with the OD77 initial conditions and the landing site location. Events along the trajectory are also indicated. Position and velocity uncertainties are shown in Figure 9. The planet-relative velocity magnitude and flight path angle are shown in Figure 10. The reconstructed initial relative flight path angle at t_0 is -13.162 deg. The reconstructed velocity magnitude at touchdown is 2.5 m/s.

The vehicle body Euler angles relative to the North-East-Down frame along with the total attitude uncertainty are shown in Figure 11. It is apparent here that the vehicle developed a roll rate during the atmospheric entry. Potential causes for this roll rate are explored in [19]. The total attitude uncertainty is shown in 11(d).

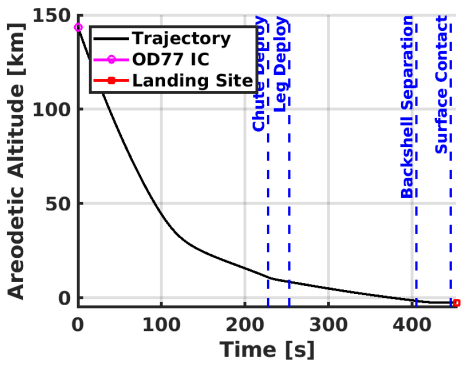

(a) Areodetic Altitude

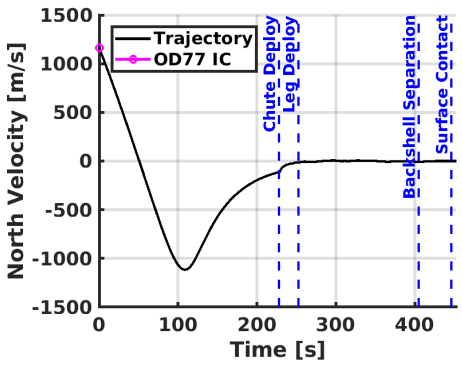

(b) North Velocity

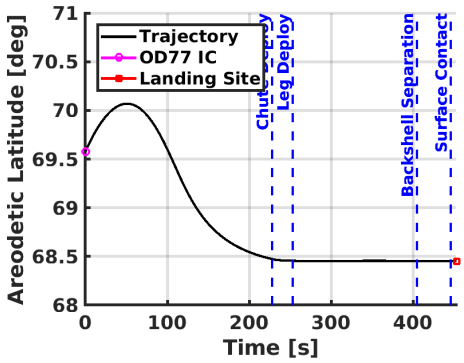

(c) Areodetic Latitude

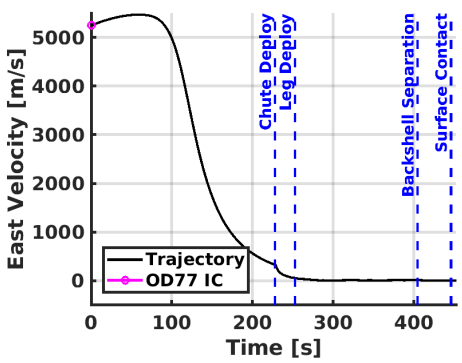

(d) East Velocity

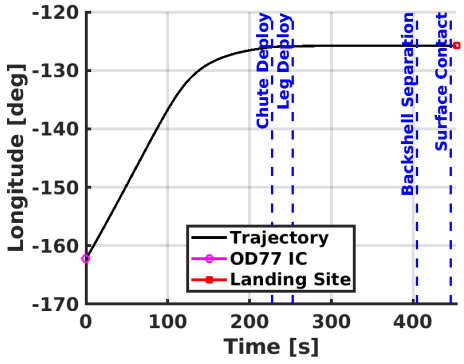

(e) Longitude

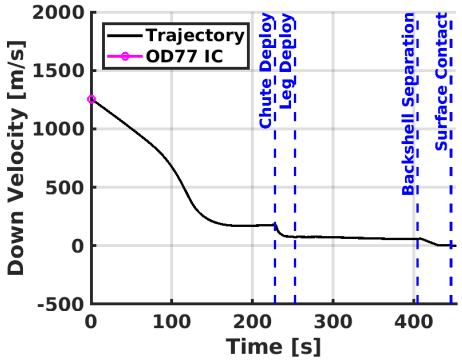

(f) Down Velocity

Figure 8: Position and Velocity

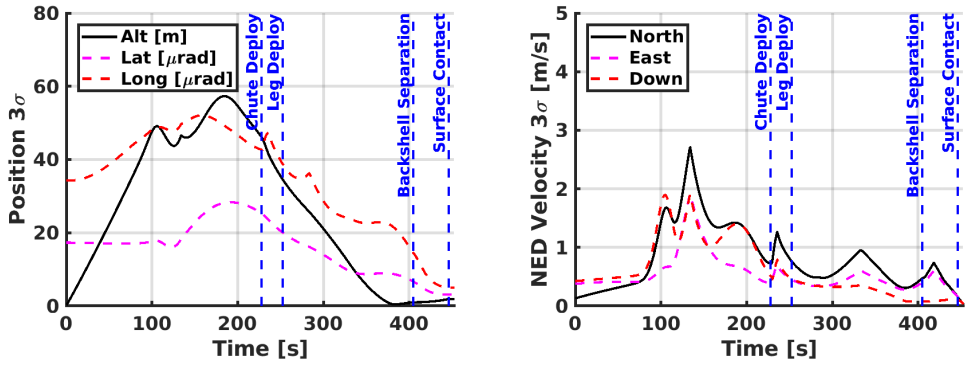

(a) Position

(b) Velocity

Figure 9: Position and Velocity Uncertainties

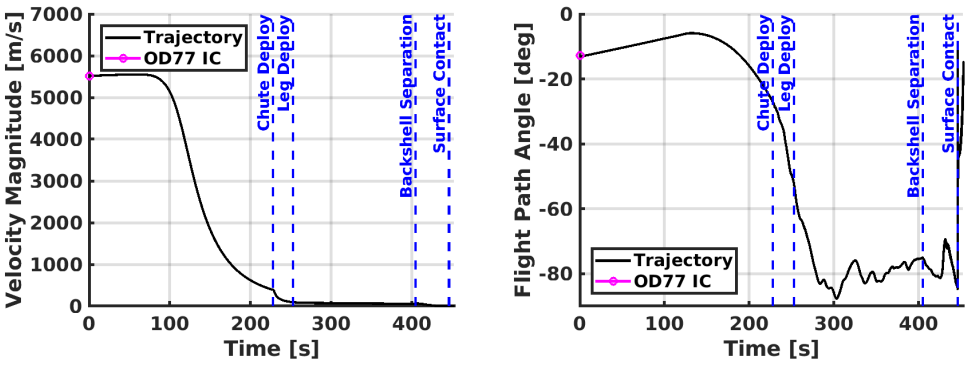

(a) Velocity Magnitude

(b) Flight Path Angle

Figure 10: Velocity and Flight Path Angle

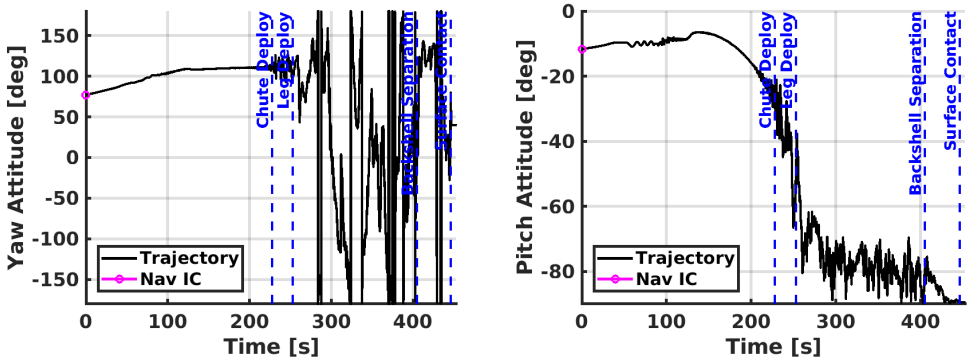

(a) Yaw

(b) Pitch

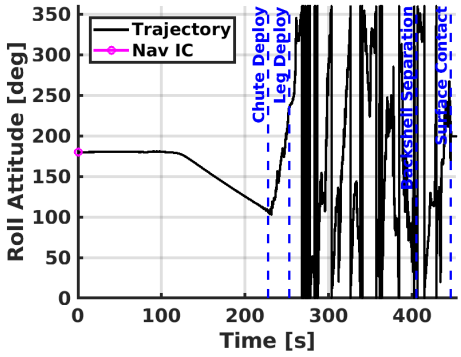

(c) Roll

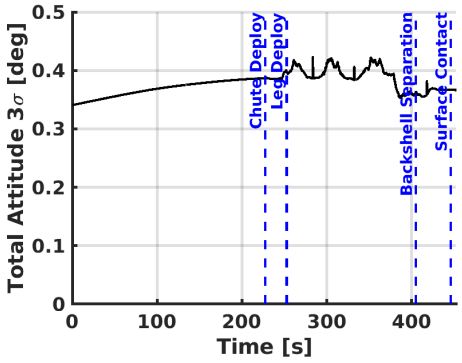

(d) Uncertainty

Figure 11: Attitude

5.2 Atmospheric-Relative Trajectory

This section describes the atmospheric-relative trajectory that was reconstructed from the inertial trajectory, accelerations, and the nominal aerodynamic database. Figure 12 shows the aerodynamic flow angles. Two sets of angles are shown. The first set is based on the inertial reconstructed trajectory with the nominal wind profile superimposed, labeled as IMU. The second set, labeled ADB, is based on the ratios of normal and side accelerations to the axial acceleration for determination of angle of attack and sideslip, respectively. In both cases there is clear signal that shows the hypersonic bounded instability. Slight differences in magnitudes of the two different angles can be explained by small heatshield to IMU coordinate frame misalignment on the order of 1 mil as shown in [19]. The ADB reconstructed angles are fairly noisy initially due to poor signal to noise ratio early in the trajectory where the dynamic pressure is low. The impact of the low signal to noise ratio is also evident in the ADB total angle of attack uncertainty shown in Figure 12(d).

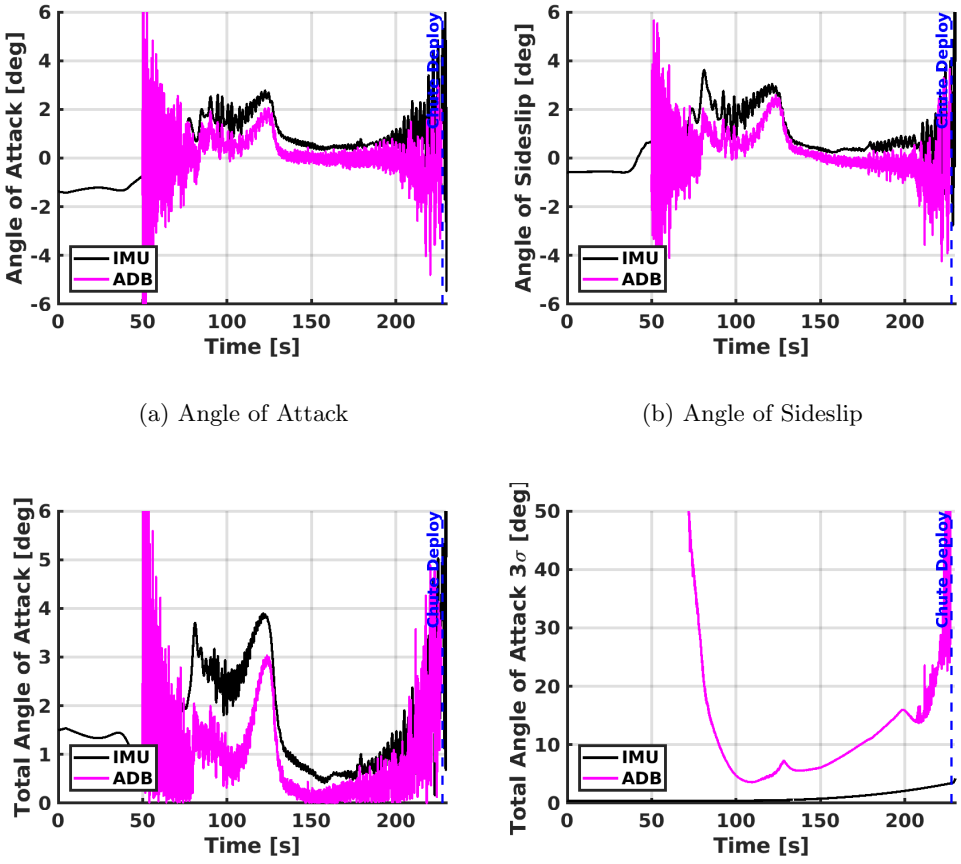

(a) Angle of Attack

(b) Angle of Sideslip

(c) Total Angle of Attack

(d) Total Angle of Attack Uncertainty

Figure 12: Aerodynamic Angles

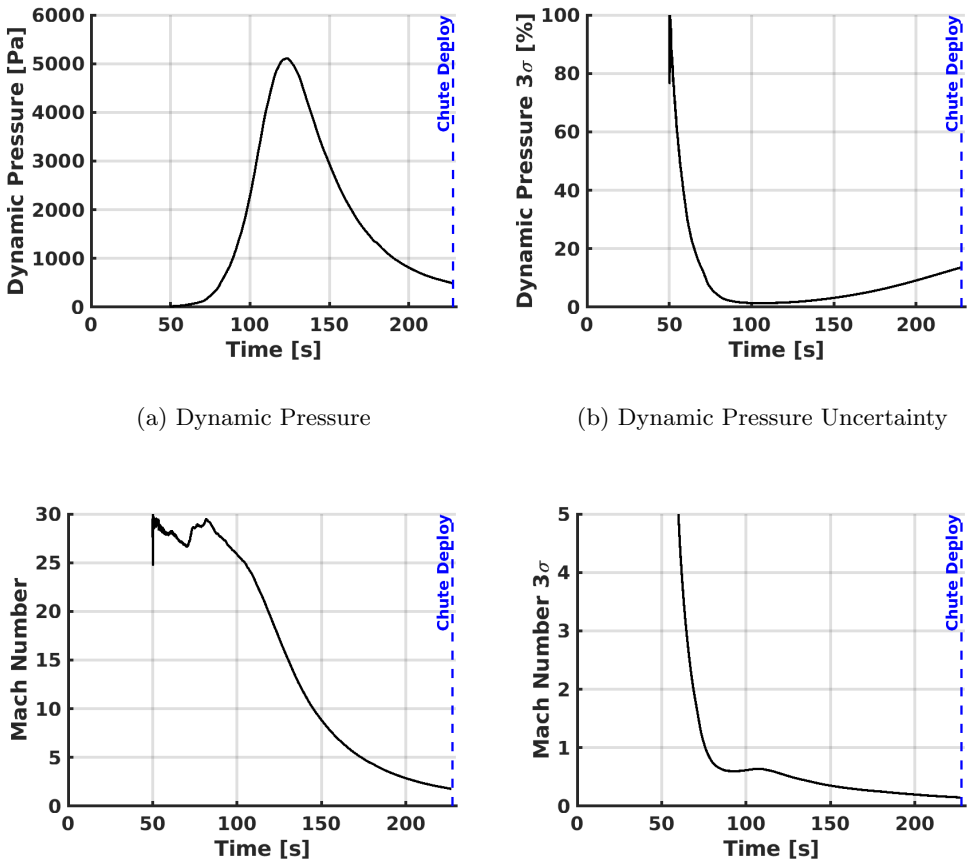

(a) Dynamic Pressure

(b) Dynamic Pressure Uncertainty

(c) Mach Number

(d) Mach Number Uncertainty

Figure 13: Atmospheric-Relative Trajectory

The reconstructed conditions at parachute deployment show a dynamic pressure of 491.5 Pa and a Mach number of 1.715. The uncertainties on these reconstructed quantities (58.6 Pa in dynamic pressure and 0.118 in Mach number, 3σ) easily encapsulates small differences between this reconstruction and other published results, such as [19].

Finally, the time histories of the atmospheric conditions along the reconstructed trajectory are shown in Figure 14. Here, the density was reconstructed from dynamic pressure and atmospheric-relative velocity (assuming the nominal wind profile). Pressure was computed from the reconstructed altitude and integration of the hydrostatic equation, and lastly temperature was computed from the ideal gas law. The next section describes the results of how these reconstructed atmospheric properties were used to generate an entry to landing as-flown atmosphere profile when combined with model data. The uncertainties of the atmospheric variables are also shown in Figure 14.

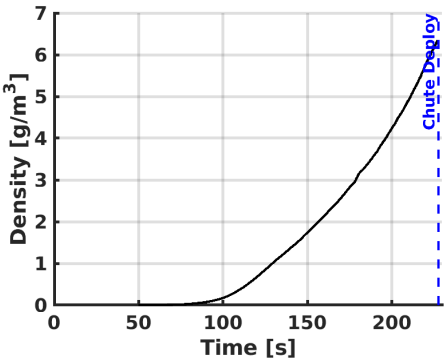

(a) Density

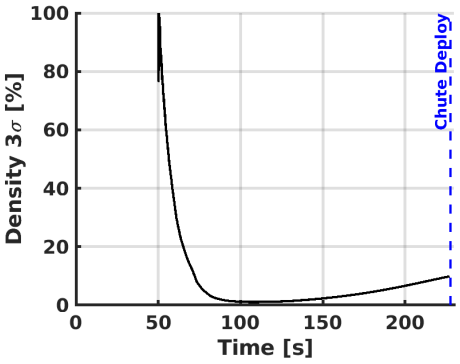

(b) Density Uncertainty

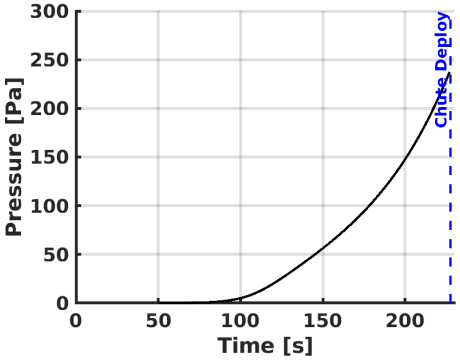

(c) Pressure

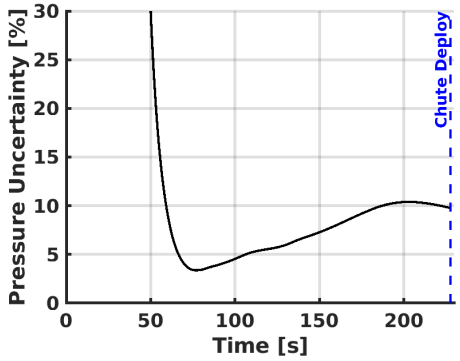

(d) Pressure Uncertainty

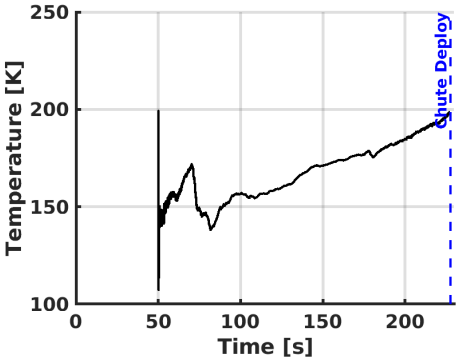

(e) Temperature

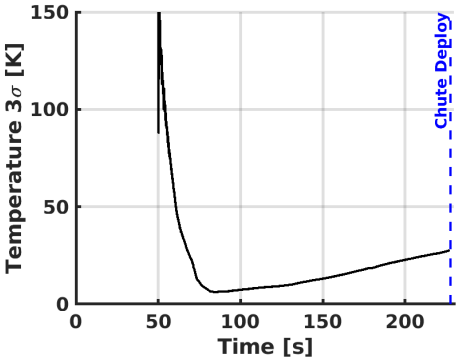

(f) Temperature Uncertainty

Figure 14: Atmosphere

5.3 Atmosphere Reconstruction

The atmospheric density profile was generated using the reconstructed density shown in Figure 14 in the altitude range between 86.6 km to 14.4 km. A best fit to the density in this altitude range was found from the 2000 dispersed cases. This dispersed density profile was used above 86.6 km and below 14.4 km. The pressure profile was computed by integrating the hydrostatic equation from an altitude of 200 km down to the landing site assuming an initial pressure of zero. The temperature profile was computed from the ideal gas law.

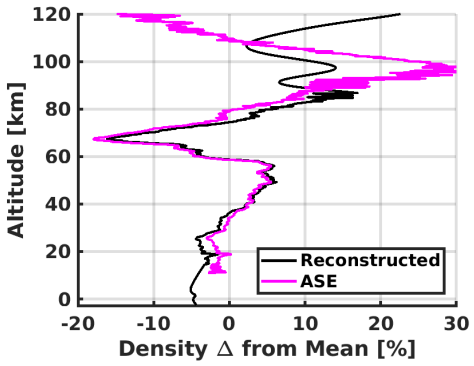

(a) Density Ratio

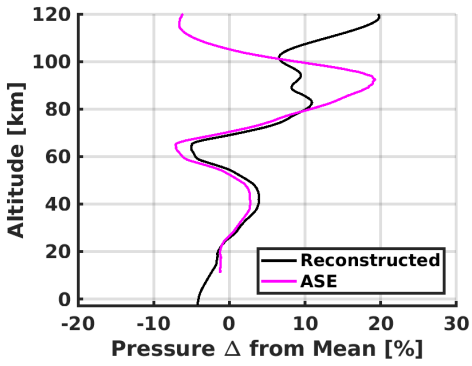

(b) Pressure Ratio

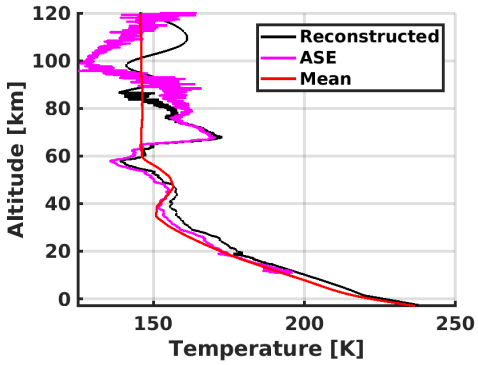

(c) Temperature

Figure 15: Comparison of Reconstructed Atmosphere to the Mean Atmosphere

A comparison of the reconstructed atmosphere to the mean atmosphere model is shown in Figure 15. Also shown for comparison are the results of the Phoenix Atmospheric Structure Experiment (ASE) documented in [23, 24]. Figure 15(a) shows the percent difference of the reconstructed density relative to the mean atmosphere profile, Figure 15(b) shows the percent difference of the reconstructed pressure, and Figure 15(c) shows the reconstructed temperature. In general the reconstructed at-

mosphere profile matches with the ASE results. Differences at upper altitudes are due to use of a dispersed atmosphere profile case above 86.6 km in the reconstructed atmosphere presented in this memorandum. The ASE data made use of accelerometer data above that altitude, although the results are noisy and so are not likely to be physically valid. Note that the ASE results end at parachute deployment and do not extend to the surface. The reconstructed temperature at the surface is 238.4 K, which matches within 0.4 K to the measurements made by the lander described in Section 3.6. The mean temperature at the surface is 234 K.

6 Trajectory Conditions

A summary of the conditions at several events in the trajectory is provided in Table 6.

Table 6: Trajectory conditions at key test events

Event	**Time from t_0** *sec*	**Mach**	**Dynamic Pressure** *Pa*	**Wind-Relative Velocity** *m/s*	**Areodetic Altitude** *km*	**Flight Path Angle** *deg*	**Total Angle Of Attack** *deg*
Initialization	0.00	27.87	0.02	5516.00	143.52	-13.16	1.53
Mach 25	104.23	25.00	3013.56	4959.23	41.46	-7.31	2.70
Mach 20	118.38	20.00	4967.75	4004.65	33.79	-6.48	3.65
Peak Deceleration	122.39	18.28	5100.33	3674.25	32.09	-6.23	3.81
Mach 15	130.29	15.00	4789.61	3036.31	29.32	-5.90	1.55
Mach 10	145.04	10.00	3344.24	2082.40	25.44	-6.24	0.67
Mach 5	173.41	5.00	1538.78	1057.88	19.98	-9.42	0.43
Parachute Deployment	227.72	1.75	492.06	391.37	10.79	-27.05	4.91
Heatshield Jettison	242.72	0.55	58.03	125.37	9.15	-39.50	8.04
Leg 1 Deployment	252.72	0.41	34.22	93.21	8.38	-52.26	6.32
Leg 3 Deployment	253.72	0.40	33.13	91.44	8.30	-54.06	16.84
Lander Separation	404.85	0.24	28.58	57.87	-1.68	-75.00	18.55
Gravity Turn	407.81	0.26	34.04	62.79	-1.86	-76.89	0.79
Touchdown	446.03	0.00	0.01	1.27	-2.64	-74.43	10.02

7 Conclusions

The NewSTEP Kalman filter trajectory reconstruction code was used to reconstruct the Mars Phoenix entry, descent, and landing trajectory and the day of landing atmosphere. All data that was available was used in the reconstruction process, including initial conditions, inertial measurement unit, radar altimeter, landing site coordinates, and atmospheric models. Uncertainties were computed on all estimated states as a by product of the Kalman filter process. The atmosphere reconstruction results compared well with published results from the Phoenix Atmosphere Structure Experiment.

References

1. Blanchard, R. C., "Mars Phoenix Mission Entry, Descent, and Landing Trajectory and Atmosphere Reconstruction," Technical Report, The George Washington University, Grant Award No. CCLS20458F, January 2009.

2. Blanchard, R. C. and Desai, P. N., "Mars Phoenix Entry, Descent, and Landing Trajectory and Atmosphere Reconstruction," *Journal of Spacecraft and Rockets*, Vol. 48, No. 5, 2011, pp. 809–821.

3. Crassidis, J. L., and Junkins, J. L., *Optimal Estimation of Dynamic Systems*, CRC Press, Boca Raton, FL, 2004, Chapter 5.

4. Grover, R. M., Cichy, B. D., and Desai, P., "Overview of the Phoenix Entry, Descent, and Landing System Architecture," *Journal of Spacecraft and Rockets*, Vol. 48, No. 5, 2011, pp. 706–712.

5. Winder, S., *Analog and Digital Filter Design, Second Edition*, Elsevier Science, 2002, Chapter 2.

6. Portock, B. M., Kruizinga, G., Bonfiglio, E., Raofi, B., and Ryne, M., "Navigation Challenges of the Mars Phoenix Lander Mission," AIAA Paper 2008–7214, August 2008.

7. Tapley, B. D., Schutz, , B. E., and Born, G. H., *Statistical Orbit Determination*, Elsevier, 2004, Chapter 2.

8. Withers, P. and Catling, D. C., "Observations of Atmospheric Tides on Mars at the Season and Latitude of the Phoenix Atmospheric Entry," *Geophysical Research Letters*, Vol. 37, 2010, Paper L24204.

9. Karlgaard C. D., Tartabini, P. V., Blanchard, R. C., Kirsch, M., and Toniolo, M. D., "Hyper-X Post-Flight-Trajectory Reconstruction," *Journal of Spacecraft and Rockets*, Vol. 43, No. 1, 2006, pp. 105–115.

10. Karlgaard, C. D., Beck, R. E., Derry, S. D., Brandon, J. M., Starr, B. R., Tartabini, P. V., and Olds, A. D., "Ares I-X Trajectory Reconstruction: Methodology and Results," *Journal of Spacecraft and Rockets*, Vol. 50, No. 3, 2013, pp. 641–661.

11. Karlgaard, C. D., Kutty, P., Schoenenberger, M., Munk, M. M., Little, A., Kuhl, C. A., and Shidner, J., "Mars Science Laboratory Entry Atmospheric Data System Trajectory and Atmosphere Reconstruction," *Journal of Spacecraft and Rockets*, Vol. 51, No. 4, 2014, pp. 1029–1047.

12. Karlgaard, C. D., Kutty, P., O'Farrell, C., Blood, E., Ginn, J., and Schoenenberger, M., "Reconstruction of Atmosphere, Trajectory, and Aerodynamics for the Low-Density Supersonic Decelerator Project," *Journal of Spacecraft and Rockets*, Vol. 56, No. 1, 2019, pp. 221–240.

13. Kutty, P. and Karlgaard, C. D., "Mars Science Laboratory Aerodatabase Trajectory Reconstruction and Uncertainty Assessment," AIAA Paper 2014-1094, January 2014.

14. Kutty, P., "Reconstruction and Uncertainty Quantification of Entry, Descent, and Landing Trajectories Using Vehicle Aerodynamics," M. S. Thesis, School of Aerospace Engineering, Georgia Institute of Technology, May 2014.

15. Rafkin, S. C. R., Haberle, R. M., and Michaels, T. I., "The Mars Regional Atmospheric Modeling System: Model Description and Selected Simulations," *Icarus*, Vol. 151, No. 2, 2001, pp. 228-256.

16. Tamppari, L. K., Barnes, J., Bonfiglio, E., Cantor, B., Friedson, A. J., Ghosh, A., Grover, M. R., Kass, D., Martin, T. Z., Mellon, M., Michaels, T., Murphy, J., Rafkin, S. C. R., Smith, M. D., Tsuyuki, G., Tyler, D., and Wolff, M., "Expected Atmospheric Environment for the Phoenix Landing Season and Location," *Journal of Geophysical Research*, Vol. 113, No. E10, 2008, Paper E00A20.

17. Prince, J. L., Desai, P. N., Queen, E. M., and Grover, M. R., "Mars Phoenix Entry, Descent, and Landing Simulation Design and Modeling Analysis," *Journal of Spacecraft and Rockets*, Vol. 48, No. 5, 2011, pp. 756–764.

18. McCleese, D. J., Schofield, J. T., Taylor, F. W., Calcutt, S. B., Foote, M. C., Kass, D. M., Leovy, C. B., Paige, D. A., Read, P. L., and Zurek, R. W., "Mars Climate Sounder: An Investigation of Thermal and Water Vapor Structure, Dust and Condensate Distributions in the Atmosphere, and Energy Balance of the Polar Regions," *Journal of Geophysical Research*, Vol. 112, No. E5, 2007, Paper E05S06.

19. Desai, P. N., Prince, J. L., Queen, E. M., Schoenenberger, M., Cruz, J. R., and Grover, M. R., "Entry, Descent, and Landing Performance of the Mars Phoenix Lander," *Journal of Spacecraft and Rockets*, Vol. 48, No. 5, 2011, pp. 798–808.

20. Taylor, P. A., Catling, D. C., Daly, M., Dickinson, C. S., Gunnlaugsseon, H. P., Harri, A., and Lange, C., "Temperature, Pressure, and Wind Instrumentation in the Phoenix Meteorological Package," *Journal of Geophysical Research*, Vol. 113, No. E3, 2008, Paper E00A10.

21. Edquist, K. T., Desai, P. N., and Schoenenberger, M., "Aerodynamics for Mars Phoenix Entry Capsule," *Journal of Spacecraft and Rockets*, Vol. 48, No. 5, 2011, pp. 713–726.

22. Konopliv, A. S., Asmar, S. W., Folkner, W. M., Karatekin, O., Nunes, D. C., Smrekar, S. E., Yoder, C. F., and Zuber, M. T., "Mars High Resolution Gravity Fields from MRO, Mars Seasonal Gravity, and Other Dynamical Parameters," *Icarus*, Vol. 211, No. 1, 2011, pp. 401–428.

23. Withers, P. and Catling, D. C., "The Phoenix Atmospheric Structure Experiment (ASE): Data Processing and Scientific Results," International Planetary Probe Workshop, Barcelona, Spain, June 2010.

24. Withers, P., Catling, D. C., and Murphy, J. R., "Phoenix Lander Atmospheric Structure Reduced Data Records, Version 1.0," PHX-M-ASE-5-EDL-RDR-V1.0, NASA Planetary Data System, Washington, D.C., 2010.

REPORT DOCUMENTATION PAGE	Form Approved OMB No. 0704–0188

1. REPORT DATE *(DD-MM-YYYY)*	2. REPORT TYPE	3. DATES COVERED *(From - To)*
01-05-2019	Technical Memorandum	

4. TITLE AND SUBTITLE
Mars Phoenix EDL Trajectory and Atmosphere Reconstruction Using NewSTEP

5a. CONTRACT NUMBER

5b. GRANT NUMBER

5c. PROGRAM ELEMENT NUMBER

6. AUTHOR(S)
Christopher D. Karlgaard and Jake A. Tynis

5d. PROJECT NUMBER

5e. TASK NUMBER

5f. WORK UNIT NUMBER
336763.01.04.15

7. PERFORMING ORGANIZATION NAME(S) AND ADDRESS(ES)
NASA Langley Research Center
Hampton, Virginia 23681-2199

8. PERFORMING ORGANIZATION REPORT NUMBER
L–21028

9. SPONSORING/MONITORING AGENCY NAME(S) AND ADDRESS(ES)
National Aeronautics and Space Administration
Washington, DC 20546-0001

10. SPONSOR/MONITOR'S ACRONYM(S)
NASA

11. SPONSOR/MONITOR'S REPORT NUMBER(S)
NASA/TM–2019–220282

12. DISTRIBUTION/AVAILABILITY STATEMENT
Unclassified-Unlimited
Subject Category 12
Availability: NASA STI Program (757) 864-9658

13. SUPPLEMENTARY NOTES

14. ABSTRACT
This document describes the trajectory and atmosphere reconstruction of the Mars Phoenix Entry, Descent, and Landing using the New Statistical Trajectory Estimation Program. The approach utilizes a Kalman filter to blend inertial measurement unit data with initial conditions and radar altimetry to obtain the inertial trajectory of the entry vehicle. The nominal aerodynamic database is then used in combination with the sensed accelerations to obtain estimates of the atmosphere-relative state. The reconstructed atmosphere profile is then blended with pre-flight models to construct an estimate of the as-flown atmosphere.

15. SUBJECT TERMS
Mars Phoenix, Trajectory Reconstruction

16. SECURITY CLASSIFICATION OF:			17. LIMITATION OF ABSTRACT	18. NUMBER OF PAGES	19a. NAME OF RESPONSIBLE PERSON
a. REPORT	b. ABSTRACT	c. THIS PAGE			STI Information Desk (help@sti.nasa.gov)
U	U	U	UU	28	19b. TELEPHONE NUMBER *(Include area code)* (757) 864-9658